CHEMISTRY
A EUROPEAN JOURNAL

DOI: 10.1002/chem.201001990

Bulk and Surface Structure and High-Temperature Thermoelectric Properties of Inverse Clathrate-III in the Si-P-Te System

Julia V. Zaikina,[a, b, f] Takao Mori,[c] Kirill Kovnir,[b, f] Detre Teschner,[d] Anatoliy Senyshyn,[e] Ulrich Schwarz,[b] Yuri Grin,[b] and Andrei V. Shevelkov*[a]

Abstract: The creation of thermoelectric materials for waste heat recovery and direct solar energy conversion is a challenge that forces the development of compounds that combine appreciable thermoelectric figure-of-merit with high thermal and chemical stability. Here we propose a new candidate for high-temperature thermoelectric materials, the type-III $Si_{172-x}P_xTe_y$ cationic clathrate, in which the framework is composed of partially ordered silicon and phosphorus atoms, whereas tellurium atoms occupy guest positions. We show that the utmost stability of this clathrate (up to 1500 K) in air is ensured by the formation of a nanosized layer of phosphorus-doped silica on the surface, which prevents further oxidation and degradation. As-cast (non-optimized) Si-P-Te clathrates display rather high values of the thermoelectric figure-of-merit ($ZT = 0.24$–0.36) in the temperature range of 700–1100 K. These ZT values are comparable to the best values achieved for the properly doped transition-metal-oxide materials. The methods of the thermoelectric efficiency optimization are discussed.

Keywords: clathrates · neutron diffraction · thermal stability · thermoelectric materials · Zintl phases

Introduction

The growing need for alternative energy sources demands new and better materials for energy generation, storage, and conversion. Thermoelectric materials (TM) that convert heat into power can be of high-impact value for wide ranging applications in Freon-free refrigerators, waste-heat converters, and direct solar thermal energy converters, as soon as efficient materials emerge.[1–4] For possible waste-heat and solar energy applications, there is a large incentive to develop thermoelectric materials that can function at elevated temperatures without degradation, displaying high thermal stability and air-oxygen resistance.[5] The performance of a thermoelectric material is expressed by the dimensionless figure-of-merit ZT. A number of modern materials display a ZT slightly exceeding 1. Materials with higher ZT, up to 2 and even higher, are expected to be developed for various applications in the coming years based on the phonon glass–electron crystal approach,[6] reflecting the intrinsic properties of the materials and nanostructuring[2,7] and employing, in addition to the latter, the surface of the particles and their interfaces for thermoelectric activity. Traditional thermoelectric materials are complex bismuth and lead tellurides and various binary and ternary antimonides.[2–4] Recently several classes of materials were scrutinized with respect to their thermoelectric applications: skutterudites,[8]

[a] Dr. J. V. Zaikina, Prof. Dr. A. V. Shevelkov
Chemistry Department, Lomonosov Moscow State University
Leniskie Gory, 1-3, Moscow 119991 (Russia)
Fax: (+7) 495-939-4788
E-mail: shev@inorg.chem.msu.ru

[b] Dr. J. V. Zaikina, Dr. K. Kovnir, Priv.-Doz. Dr. U. Schwarz, Prof. Yu. Grin
Max-Planck-Institut für Chemische Physik fester Stoffe
Nöthnitzer Str., 40, Dresden 01187 (Germany)

[c] Dr. T. Mori
MANA, National Institute for Materials Science
Namiki 1-1, Tsukuba 305-0044 (Japan)

[d] Dr. D. Teschner
Fritz-Haber-Institute of the Max-Planck Society
Faradayweg 4-6, Berlin, 14195 (Germany)

[e] Dr. A. Senyshyn
Forschungsneutronenquelle Heinz Maier-Leibnitz (FRM II)
Technische Universität München
Lichtenbergstrasse 1, D-85747 Garching bei München (Germany)

[f] Dr. J. V. Zaikina, Dr. K. Kovnir
Present address: Department of Chemistry and Biochemistry
Florida State University, Chieftan Way 95
Tallahassee, FL, 32306 (USA)

Supporting information for this article is available on the WWW under http://dx.doi.org/10.1002/chem.201001990.

clathrates,[3,4,9] Zn_4Sb_3,[10] $Yb_{14}MnSb_{11}$,[11] and others. The best optimized materials of these classes have appreciable thermoelectric performance with $ZT>1$ at different temperatures ranging from 300 to 1000 K, although these materials are not stable in air at elevated temperature. To develop thermoelectric materials with greater stability in air in the temperature region above 900 K, compounds such as boron carbide ($ZT_{1000K}=0.25$),[12] Si–Ge alloys ($ZT_{1000K}=0.6$ for p-type),[13] various complex oxides ($ZT_{1000K}=0.3$),[14] and recently, newly designed boron cluster-based compounds ($ZT_{1000K}=0.12$)[15] are being extensively studied.

Zintl clathrates are an interesting class of compounds studied for possible thermoelectric applications, since they display low thermal conductivity coupled with relatively large thermoelectric power and electrical conductivity, the necessary conditions for high thermoelectric efficiency.[9c,16–18] Type-I, type-II, type-VIII, and type-IX clathrates were extensively investigated in view of possible thermoelectric applications.[3,4,9] The thermoelectric properties of any clathrate-III compounds have not been reported so far. Additional drawback of conventional clathrates are the relatively low melting points, which are, in general, not as high as the previously mentioned systems and also, the clathrates corrosion resistance to air is rather insufficient.[19–21] In contrast, the recently discovered Si-P-Te clathrate-III exhibits one of the highest known melting points among clathrates, at about 1500 K, and is stable in air at least below 1500 K.[22]

In this paper, we discuss the reasons for the utmost stability of clathrate-III in air and show that it is ensured by the formation of a nanosized layer of phosphorus-doped silica on the surface, which prevents further oxidation and degradation. We also report the high-temperature thermoelectric properties of Si-P-Te clathrate-III and compare them with the properties of the type-I Si-P-Te clathrate.[23] We also show that the non-optimized Si-P-Te clathrates display intriguing values of the thermoelectric figure-of-merit ($ZT=$ 0.24–0.36) in the temperature range of 700–1100 K, emphasizing high prospects of developing effective thermoelectric materials for heat-waste recovery and direct solar energy conversion at elevated temperatures. The degree of disorder in the crystal structure of the clathrate-III is probed with neutron diffraction. The vast impact of the composition and atomic arrangements of Si-P-Te clathrate-I and clathrate-III on their thermoelectric properties is discussed.

Results and Discussion

Clathrate-III $Si_{131.8(3)}P_{40.4(4)}Te_{21.5(1)}$ and reference clathrate-I $Si_{31.9(1)}P_{13.9(1)}Te_{7.00(3)}$ were prepared by a standard ampoule technique as described in detail elsewhere.[22,23d] XRD data yield the unit cell parameters: $a=9.9772(1)$ Å for the cubic $Si_{31.9(1)}P_{13.9(1)}Te_{7.00(3)}$, and $a=19.2491(4)$ Å and $c=$ 10.0706(3) Å for the tetragonal $Si_{131.8(3)}P_{40.4(4)}Te_{21.5(1)}$, which appeared to be in excellent agreement with our previous results.[22,23d] The phase compositions were confirmed by energy dispersive X-ray spectroscopy (EDXS) and wavelength dispersive X-ray spectroscopy (WDXS), and the quality of the specimens was checked by a combination of metallographic investigations, SEM and WDXS, as well as by powder XRD. Lab-scale (up to 2 g) samples of both clathrates can be prepared as single phase materials. Large-scale samples (≈5 g) of clathrate-I were proved to be single phase, whereas the large-scale samples of clathrate-III used for thermoelectric measurements contained only a minor impurity of the clathrate-I.

The Si-P-Te clathrates are members of a large family of cage compounds,[24] in which the framework built of silicon and phosphorus atoms traps tellurium anions inside the cages. Only two types of polyhedral cages with 20 and 24 vertices are present in the clathrate-I structure in the 2:6 ratio per unit cell. The crystal structure of clathrate-III is more complex; it exhibits three different cages with 20, 24, and 26 vertices alternating in a unit cell in a 10:16:4 ratio per unit cell (Figure 1). The largest 26-vertex polyhedra are

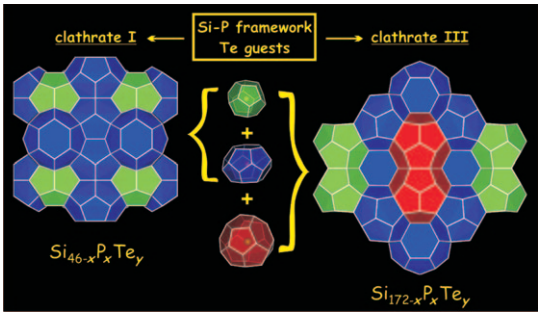

Figure 1. Polyhedral representation of the crystal structures of the type-I (left) and type-III (right) clathrates. 20-vertex polyhedra, green; 24-vertex polyhedra, blue; 26-vertex polyhedra, red.

unique and are not present in other clathrate types. For a matter of clarity, hereafter, "type-I clathrate" is used for the sample with the composition $Si_{32}P_{14}Te_7$ and "type-III clathrate" for $Si_{132}P_{40}Te_{21.5}$, which represents the compositions from the homogeneity ranges for the corresponding clathrates. Both crystal structures feature mixing of silicon and phosphorus atoms on different sites of the clathrate framework and contain vacancies in the guest tellurium positions. In both structures guest tellurium atoms occupy only a part of the 20-vertex cages, 15% in $Si_{132}P_{40}Te_{21.5}$ and 50% in $Si_{32}P_{14}Te_7$.[22,23d] According to their crystal structures, these clathrates are expected to have properties of a "phonon glass–electron crystal", which means that the covalently bonded clathrate framework ensures the efficient transport of charge carriers, while the guest atoms inside the oversized cages scatter heat-carrying phonons.[21,25]

Neutron diffraction: For thermoelectric materials, the local and/or long-range disorder plays a very important role.[10,26] For clathrates, it is generally believed that low thermal conductivity is due to rattling of the guest atoms in the oversized cages. However, local disorder in the clathrate framework should not be neglected.[27] We have shown by means

of neutron diffraction and solid-state NMR spectroscopy that Si-P-Te clathrate-I exhibits a high degree of disorder associated with mixed occupation of most of the framework positions by Si and P atoms.[23d] Clathrate-III represents a more complicated crystal structure with 17 framework positions, each of which may be occupied either by P, or Si, or both. X-ray single crystal analysis did not allow us to unambiguously determine the framework structure due to similar scattering factors of Si and P. Based on the analysis of interatomic distances and ^{31}P NMR spectroscopy studies, lower framework disorder was proposed for Si-P-Te clathrate-III compared with clathrate-I.[22] Two of 17 positions were suggested to be fully occupied by phosphorus, P(1) and P(2), and three other positions E(3), E(4), and E(5) were set to be occupied by a mixture of Si/P. The Si/P ratio in these positions was fixed to 0.55/0.45 to achieve the experimentally determined composition by WDXS.[22]

To prove the Si/P distribution we performed neutron powder diffraction studies (Figure 2), since Si and P have different neutron coherent scattering lengths (5.13 fm for P and 4.15 fm for Si). During the refinement, the occupancy of each framework position was allowed to vary. The results of the Rietveld refinement of neutron data confirms the model proposed on the basis of X-ray single crystal data (Tables S1 and S2 in the Supporting Information). The positions P(1) and P(2) are fully occupied by phosphorus, whereas the positions E(4) and E(5) feature mixed occupation with the Si/P ratios of 0.43(2)/0.57 and 0.59(2)/0.41, respectively. The only differences in the Si/P assignment derived from neutron data compared with that from the single-crystal XRD are the positions E(3) and Si(17). According to the neutron data refinements, the 8-fold position E(3) is fully occupied by silicon, whereas the 16-fold position Si(17) has mixed Si/P occupancy with the 0.80(2)/0.20 ratio. Thus, the neutron powder diffraction allowed us to unambiguously establish the distribution of Si and P over the clathrate-III framework positions (Figure 3). The analysis of the local coordination of Te atoms reveals that phosphorus atoms prefer to build the smaller pentagonal-dodecahedral

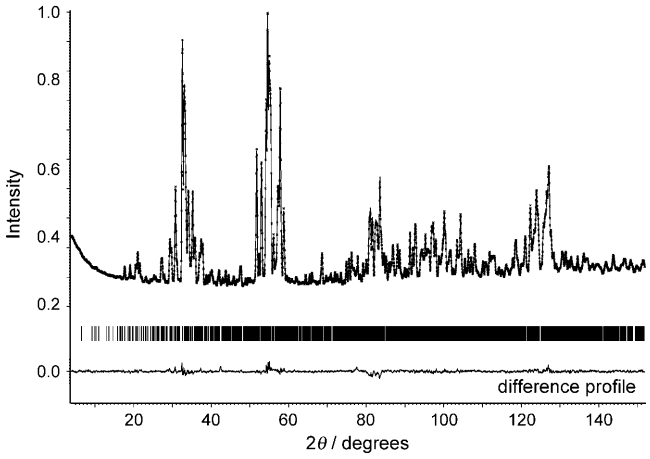

Figure 2. Neutron diffraction Rietveld plot for the refinement of the clathrate-III, experimental data (crosses), calculated profile (line), and difference profile (lower part) are shown.

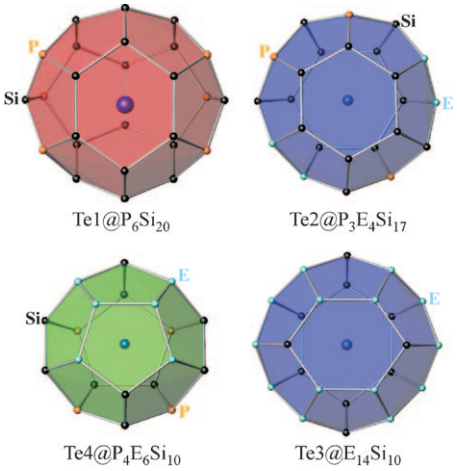

Figure 3. Coordination of Te atoms in the crystal structure of Si-P-Te clathrate-III. The sizes of the spheres are proportional to isotropic ADP. Si: black; P: orange; E = Si/P: green; Te: blue.

cage, in which 10 atoms of 20 are either P or E (= Si/P). The 24-vertex polyhedra contain either 7 or 14 P and E atoms, whereas the largest 26-vertex cage contains only six P atoms. The latter Te cage (diameter of 7.2 Å) is unique to clathrate-III and is not present in type-I, II, VIII, or IX clathrates. The tellurium atom inside this polyhedron shows remarkably higher atomic displacement parameters (ADP) (Figure 3). The refinement of the occupancy of Te(1) did not reveal any deviations from 100%. The ADPs in the clathrate structure are attributed to the rattling of the guest atom within the oversized cage, which is one of the key conditions for low thermal conductivity necessary for efficient thermoelectric material.[9,21,25]

Surface oxidation: To investigate the utmost thermal stability of the Si-P-Te clathrates the X-ray photoelectron spectroscopy (XPS) studies were performed on a single-phase sample of clathrate-III. The sintered ingot of the sample was divided into two parts. One of these was investigated as cast, without any further treatment, whereas another part was annealed in air at 1273 K for 30 min. The XRD patterns were identical for both parts, without significant changes of the unit cell parameters (Figure S1 in the Supporting Information). XPS investigation based on the synchrotron source has the following advantage: the wavelength of the incoming radiation may be varied to probe the surface depth profile of the material.[28] In current studies, Te3d, P2p, Si2p, and C1s XP spectra were recorded with different primal beam wavelengths resulting in photoelectrons with similar kinetic energy. Thus, the same information depth was probed for each element. Three different kinetic energies were chosen: 780, 380, and 150 eV. These correspond to in-

formation depths (three-times the inelastic mean free path) of about 6, 3.5, and 2 nm, respectively, for clean $Si_{131.8}P_{40.4}Te_{21.5}$.[29]

The $Te3d_{5/2}$ XP spectrum recorded at the highest kinetic energy (i.e., highest information depth, most bulk-sensitive mode) clearly indicates a negative oxidation state for tellurium in clathrate-III (Figure 4). The binding energy (BE) of

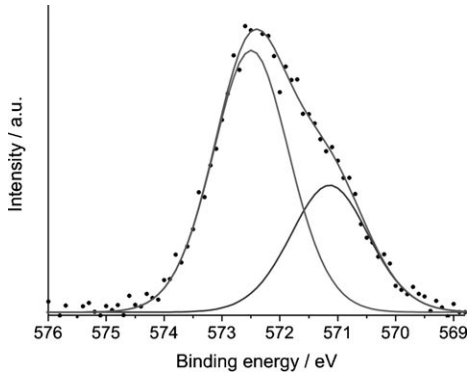

Figure 4. $Te3d_{5/2}$ region of the XPS for the as-cast sample of the type-III clathrate $Si_{1312}P_{40}Te_{21.5}$; $h\nu = 1350$ eV.

elemental tellurium is 572.9 eV, whereas Te in positive oxidation states has significantly higher binding energies, above 575 eV.[30] The obtained spectrum can be deconvoluted into two components with binding energies 571.1 and 572.5 eV (Table 1). The lower value is similar to the BE reported for

Table 1. Results of the XPS investigation of the clathrate-III $Si_{132}P_{40}Te_{21.5}$.[a]

	As cast		Anneal. at 1273 K	
	Peak [eV]	Rel. intensity	Peak [eV]	Rel. intensity
Si^0	100.0	12%	100.5	5%
Si^{+4}	103.6	88%	103.8	95%
P^0	129.6	42%	Not detectable	
P^{+5}	134.9	58%	134.8	weak
Te^{2-}	571.1	33%	Not detectable	
Te^0	572.5	67%		

[a] Photoelectron kinetic energy = 780 eV. It corresponds to a clathrate information depth of ≈6 nm and a silica information depth of ≈7.3 nm, calculated as approximately triple the inelastic mean free path of photoelectrons with such kinetic energy in the material.[29]

A_2Te (A = K, Cs) films (BE = 571.1–571.5 eV) in which the oxidation state −2 can be assumed for tellurium.[31] The BE of the higher component is close to elemental tellurium.[30,31] An explanation for the two components might be that Te atoms in different types of polyhedral cages in the crystal structure of clathrate III exhibit dissimilar charges. However, the observed Te3d peak component ratio of 1:2 does not correlate with the cage occupancies in the crystal structure, in which the calculated ratio of tellurium atoms occupying cages with 26, 24, and 20 vertices is 4:16:1.2.[22] The most probable reason is a partial oxidation of the sample on the surface. The latter assumption is supported by the fact that in the surface-sensitive mode only one component in the $Te3d_{5/2}$ spectrum with a binding energy of 572.7 eV was detected. A similar observation was reported for A_2Te (A = K, Cs) films in which a moderate oxidation or deficiency of alkali metal led to the elimination of the low binding energy component and to the formation of a new component with the BE close to that of elemental tellurium. Such a BE was still attributed to $Te^{\delta-}$.[31] Thus, in the bulk structure of clathrate-III, tellurium has an oxidation state of −2 while on the surface it is partially oxidized.

Investigations of silicon and phosphorus XP spectra support the assumption of partial surface oxidation (Table 1). For each element two well-resolved components were obtained. In the case of phosphorus the low BE (129.6 eV) component is close to that reported for elemental phosphorus or for covalent phosphides, such as MP (M = Ga, In), whereas the higher BE component (134.9 eV) represents the completely oxidized P^{+5} in metaphosphates and P_4O_{10}.[30] Similarly, for Si the low BE of 100 eV corresponds to the elemental silicon or covalently bonded silicon in silicon carbide, SiC, whereas the higher BE of 103.6–103.9 eV is typical for silica.[30] In surface sensitive mode the intensity of elemental peaks decrease with a concomitant development of oxide peaks. Therefore, the XPS results conform to the simple, yet powerful, Zintl concept,[32] that is, in the bulk structure of Si-P-Te clathrates, the Te atoms realize an electron octet by accepting electrons from the framework atoms, thus becoming Te^{2-}, whereas Si and P atoms achieve the close-shell configuration by forming four covalent bonds each and having oxidation states close to zero. Additionally, the XPS investigations of clathrate-III show that its surface is partially oxidized, since mainly P^{+5} and Si^{+4} were detected at an information depth of 2 nm. The thickness of the oxide coating can be estimated from the penetration depth as ≤5 nm.

Temperature treatment of clathrate-III in air at 1273 K leads to no bulk oxidation or decomposition as detected by powder XRD. However, the XPS indicates a significant alteration of the surface. After temperature treatment, the XP spectrum revealed no Te in the near-surface region of the sample independently on independent of the wavelength of the incoming radiation used. A very weak phosphorus signal was present in a bulk sensitive mode and the corresponding BE indicates the oxidation state +5. Clearly, the main XP signal arises from silica, BE = 103.8 eV (Table 1). At two other kinetic energies used (i.e., in surface-sensitive mode), only the silica signal was detected at similar BE and neither P nor Te were present. Thus, the rearrangement of the oxide layer on the surface of the type-III clathrate occurs due to the high-temperature treatment in air resulting in the formation of a silica top layer with a thickness of about 7 nm. Similar behavior was previously reported for some metal silicides.[33] For Si-P-Te clathrates, such a silica coating has a high impact on the stability of the studied compounds in air, protecting them from further oxidation.

Thermoelectric properties: For the reason of comparison, the TM properties of Si-P-Te clathrate-III were studied together with those of clathrate-I. A brief report of the thermoelectric properties of the Si-P-Te clathrate-I sample with unascertained composition and containing a significant amount of impurities was reported recently.[23b] However, the composition, the distribution of atoms over the framework positions and the occupancies of the guest positions were not determined, which hampered the establishment of the structure–property relationship. In our work, we studied the well-defined single-phase sample of clathrate-I with the composition $Si_{31.9(1)}P_{13.9(1)}Te_{7.00(3)}$.

The temperature dependence of the resistivity (ρ), Seebeck coefficient (α), power factor (P), and thermal conductivity (κ) of the type-III and type-I Si-P-Te clathrates are plotted in Figure 5a–d. Notable are the very low absolute values of the resistivity for the type-I compound, with $\rho <$ 100 μΩm across the whole temperature range. There is some scatter, but in general the dependence appears to be an increase in ρ as the temperature is increased. The type-III clathrate shows sizably higher resistivity, with the room temperature value larger by about a factor of four. Interesting temperature dependence is observed with the resistivity showing a precipitous decrease above 1000 K. Both compounds are p-type conductors, since the values of the Seebeck coefficient are positive in the whole range of measurements. In contrast to the low values of resistivity, the Seebeck coefficients are quite large, with $\alpha > 200\ \mu V K^{-1}$ above 550 K for both compounds. Charge carriers transported in TM materials are characterized by the power factor $P = \alpha^2/\rho$ (Figure 5c). According to the Zintl concept,[32] type-I and type-III Si-P-Te clathrates are quite different. For type-I clathrates $Si_{46-x}P_xTe_y$, small deviations from the Zintl composition, that is, $x < 2y$, were detected, which implies heavily doped semiconductor properties.[23d] In turn, clathrate-III $Si_{172-x}P_xTe_y$ has the exact Zintl composition ($x = 2y$) and exhibits typical semiconducting behavior.[22] Thus, the power factor for a type-I clathrate is expected to be higher compared with that of clathrate-III in the whole temperature range. At 1000 K the absolute values of P are $1000\ \mu W K^{-2} m^{-1}$ and $120\ \mu W K^{-2} m^{-1}$, respectively. Although a maximum in the power factor is reached at 1000 K for the type-I clathrate, P increases sharply for the type-III clathrate above 1000 K. In general, for TM materials high power factors are required until the charge carriers contribution to thermal conductivity remains essentially small compared with the phonon contribution.

The thermal conductivity of both types of clathrate decreases with temperature, but then undergoes a broad minimum around 600 K and increases (Figure 5d). It is significantly smaller for clathrate-III compared with clathrate-I in the whole temperature range. The total thermal conductivity κ comprises the electronic thermal conductivity, κ_e, and the contribution from the lattice, κ_L.[34] As expected from the higher power factor, κ_e is higher for clathrate-I, with the maximum value of $0.30\ W m^{-1} K^{-1}$ (Figure 5d), whereas it does not exceed $0.15\ W m^{-1} K^{-1}$ for the type-III sample (not shown). In both cases the electronic contribution constitutes not more than 15% of the total thermal conductivity, mean-

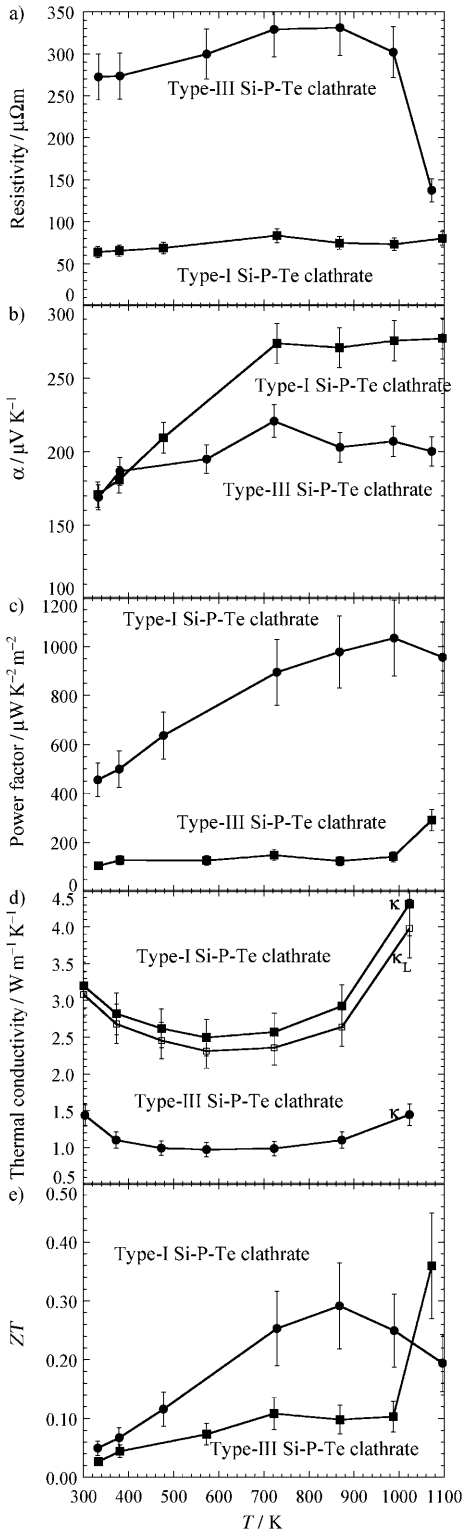

Figure 5. Temperature dependence of a) the resistivity; b) Seebeck coefficient; c) power factor; d) total thermal conductivity, κ, and lattice thermal conductivity, κ_L; e) figure-of-merit for type-I and type-III Si-P-Te clathrates. Error bars are included; the lines running through the data points are guides to the eye.

ing that the lattice part is dominant. Clathrate-III has large oversized 26-vertex cages with Te trapped inside such polyhedra. These Te atoms exhibit extremely high rattling as can be concluded form the X-ray[22] and neutron diffraction data (see above). In turn, the degree of framework disorder, for example, joint occupancy of one atomic position by Si/P, is lower for clathrate-III compared with clathrate-I as evidenced from the neutron diffraction data. We conclude that the rattling of the guest atoms affects the phonon transport greater than the Si/P disorder, which contributes less because these light atoms have close atomic numbers and evoke only minor mass alternation.

The dimensionless figure-of-merit $ZT = PT/\kappa$ (Figure 5e) was calculated assuming a smooth extrapolation of κ to 5.4 $Wm^{-1}K^{-1}$ at 1100 K for the type-I clathrate and to 1.65 $Wm^{-1}K^{-1}$ for the type-III one. For the type-I clathrate ZT reaches a maximum value of approximately 0.30 at 870 K, whereas it sharply increases for the type-III clathrate after 1000 K reaching $ZT = 0.36$ at 1100 K. These figures-of-merit values are still lower than those for the air-stable doped p-type Si_xGe_{1-x} bulk alloy ($ZT \approx 0.6$),[13] but are comparable to the best ZT values at the respective temperatures (1000 K) achieved for optimized oxide materials ($ZT \approx 0.3$).[14] These materials are the only known thermoelectrics stable in air at temperatures of about 1000 K; their performance has been intensively optimized, and these values can be used as a benchmark for air-resistant thermoelectric materials. Though higher ZT values were reported for several compounds at very high temperatures, for example $Yb_{14}MnSb_{11}$ with $ZT = 1.05$ at the highest temperature of 1250 K,[11] their chemical instability towards oxidation in air is a barrier for their wide-spread application as power generators.

Considering that this is the first report on the TM properties of the type-III clathrate, for the "as-cast", non-optimized compound, the ZT values obtained in this work are promising. The clathrate structure offers exceptional ways for optimization of thermoelectric parameters, allowing us to tune the resistivity and thermal conductivity almost independently of each other. The optimization pathways stem from the results of the current work. Proper doping of a Si–P framework of clathrate-III should result in heavily doped semiconductor behavior similar to the case of clathrate-I. This would raise the power factor without significant affect on the thermal conductivity. Thus, doping of Zn into clathrate $Ba_8Ni_nGa_{16-m}Ge_{46-n-m}$ resulted in a fourfold increase of ZT up to the 1.2 value at 1000 K.[35] In turn, thermal conductivity of both type-III and type-I clathrates can be significantly lowered owing to guest atom substitution.[36] Mixing of Te with halogens or Se would result in a further decrease of thermal conductivity. The optimization studies of Si-P-Te clathrates should also prove to be of very high interest and will be reported in due course.

Conclusion

The type-III Si-P-Te clathrate with the cage-like crystal structure exhibits high chemical and thermal stability originating from the ultra-fine (undetectable with XRD) silica film that develops on the surface of the bulk sample during heating in air, which prevents further degradation of the material. Similar to type-I Si-P-Te clathrate, the type-III clathrate displays a combination of high electrical conductivity with high thermoelectric power. However, these p-type semiconductors do not exhibit low enough thermal conductivity, which is, on average, a factor of three higher than that observed in the majority of the clathrates.[18,27] Already, with such a relatively high thermal conductivity, ZT reaches promising values of 0.30 for the type-I clathrate at 870 K and 0.36 for the type-III clathrate at 1100 K. The comparison of the crystal structures of these clathrates shows that the higher ADP's of the tellurium guests in the oversized 26-vertex cages apparently leads to lower thermal conductivity of clathrate-III. These findings show that the silicon-based clathrates present a new family of prospective materials for high-temperature power generation.

Experimental Section

Synthesis and characterization: Stoichiometric mixtures of elemental Si, red P, and Te were annealed in quartz ampoules that were sealed under vacuum. A single phase sample of clathrate-I was synthesized by two-step annealing at 1375 K for 100 and 144 h with subsequent regrinding to achieve homogeneity and approach thermodynamic equilibrium.[23d] A single phase sample of clathrate-III was obtained by the annealing of elements at 1425 K for 18 days.[22] To obtain compact large scale ($\approx$5 g) samples suitable for thermoelectric measurement, the sample of clathrate-I was pressed into a pellet and annealed for a third time at 1425 K for 18 days. A large-scale sample of clathrate-III was obtained by the annealing of elements at 1425 K for 18 days.

XRD was performed in a transmission alignment by using a Huber G670 Image Plate Camera, $Cu_{K\alpha 1}$ radiation, $\lambda = 1.540598$ Å. The unit cell parameters were calculated from least-square fits using LaB_6 (cubic, $a = 4.15692$ Å) as an internal standard.

Polished samples were examined by optical microscopy (Zeiss Axioplan2) and SEM. The microstructure images were obtained in back scattering electron (BSE) contrast (Cameca SX100). The composition was determined by energy dispersive X-ray spectroscopy (EDXS) and wavelength dispersive X-ray spectroscopy (WDXS). GeTe and SiP_2 were used as standards to calibrate the tellurium, silicon, and phosphorus contents.

Neutron diffraction: Elastic coherent neutron scattering experiments were performed at the research reactor FRM-II (Garching, Germany) on the high-resolution diffractometer SPODI.[37] Monochromatic neutrons ($\lambda = 1.5475$ Å) were obtained at 155° take-off angle using the 551 reflection of a vertically-focused composite Ge monochromator. The vertical position-sensitive multidetector (300 mm effective height) consisting of 80 ^{3}He tubes and covering an angular distance of 160° 2θ was used for data collection. The studied lab-scale sample (about 0.5 cm^3 in volume) was filled into a thin-wall (0.15 mm) vanadium container of 10 mm diameter. 2D powder diffraction data were collected at ambient temperature and then corrected for geometrical aberrations. The Rietveld refinement of the neutron diffraction data was carried out by using the JANA2000 software package.[38] The peak profile shape was modeled by choosing the pseudo-Voigt function. The scale factor, lattice parameter, fractional coordinate of atoms, their isotropic displacement parameters, site occu-

pancies, zero angular shift, profile shape parameters, and half width parameters were varied during the fitting.

XPS studies: A single-phase sample of clathrate-III was used for the X-ray photoelectron spectroscopy (XPS) experiments. XPS experiments were performed at beamline ISISS at BESSY (Berlin, Germany). Samples were investigated in ultra-high vacuum (pressure $\approx 10^{-8}$ mbar) without sputtering to get information about the surface of the samples. The data were calibrated by using the C1s line arising from adventitious surface carbon contamination, the main component of the C1s line was fixed to a value of 284.7 eV. Accuracy of such a calibration can be estimated as not exceeding 0.2 eV.

Property measurements: Electrical resistivity was measured by using the four-probe method, whereas thermoelectric power was measured by a differential method in the temperature range from 300 to 1100 K in helium gas with an ULVAC ZEM-2. To determine the thermal conductivity, first of all, the room temperature specific heat was measured by using a transient heat pulse method with a small temperature increase of 2% relative to the system temperature. Then, the relative specific heat and thermal diffusivity coefficient were measured by a laser flash method from 300 to 1050 K under vacuum with an ULVAC TC-7000. The thermal conductivity is determined as the product of the density measured by a pycnometric method, the specific heat, and the thermal diffusivity coefficient. The density of all used samples exceeds 90% of their theoretical X-ray density.

Acknowledgements

The authors express their gratitude to Dr. Yu. Prots for the help with collection of neutron powder patterns, and M. Friedrich and Dr. R. Blume for assistance in collection photoelectron spectra, as well as T. Vogel, M. Eckert, and Dr. U. Burkhardt for help in metallographic, SEM, and WDXS investigations. We thank FRM II and BESSY for providing beam time and continuing support during the experiments. JVZ acknowledges the Max-Planck-Gesellschaft for a research fellowship. This work is supported in part by the Russian Foundation for Basic Research.

[1] G. S. Nolas, J. Sharp, H. J. Goldsmid in *Thermoelectrics: Basic Principles and New Materials Developments*, Springer, New York, **2001**.
[2] J. R. Sootsman, D. Y. Chung, M. G. Kanatzidis, *Angew. Chem.* **2009**, *121*, 8768–8792; *Angew. Chem. Int. Ed.* **2009**, *48*, 8616–8639.
[3] G. J. Snyder, E. S. Toberer, *Nat. Mater.* **2008**, *7*, 105–114.
[4] A. V. Shevelkov, *Uspekhi Khimii* **2008**, *77*, 3–21; A. V. Shevelkov, *Russ. Chem. Rev.* **2008**, *77*, 1–19.
[5] T. M. Tritt, H. Bottner, L. Chen, *MRS Bull.* **2008**, *33*, 366–368.
[6] G. A. Slack in *CRC Handbook of Thermoelectrics* (Ed.: D. M. Rowe), CRC Press, New York, **1995**.
[7] a) M. S. Dresselhaus, G. Chen, M. Y. Tang, R. G. Yang, H. Lee, D. Z. Wang, Z. F. Ren, J.-P. Fleurial, P. Gogna, *Adv. Mater.* **2007**, *19*, 1043–1053; b) K. Ahn, M. K. Han, J. He, J. Androulakis, S. Ballikaya, C. Uher, V. P. Dravid, M. G. Kanatzidis, *J. Am. Chem. Soc.* **2010**, *132*, 5227–5235.
[8] a) B. C. Sales, D. Mandrus, R. K. Williams, *Science* **1996**, *272*, 1325–1328; b) G. S. Nolas, M. Kaeser, R. T Littleton IV, T. M. Tritt, *Appl. Phys. Lett.* **2000**, *77*, 1855–1857.
[9] a) E. S. Toberer, A. F. May, G. J. Snyder, *Chem. Mater.* **2010**, *22*, 624–634; b) M. Beekman, G. S. Nolas, *J. Mater. Chem.* **2008**, *18*, 842–851; c) M. Christensen, S. Johnsen, B. B. Iversen, *Dalton Trans.* **2010**, *39*, 978–992.
[10] a) J. Nylén, S. Lidin, M. Andersson, B. B. Iversen, H. Liu, N. Newman, U. Häussermann, *Chem. Mater.* **2007**, *19*, 834–838; b) G. J. Snyder, M. Christensen, E. Nishibori, T. Caillat, B. B. Iversen, *Nat. Mater.* **2004**, *3*, 458–463.
[11] a) E. S. Toberer, C. A. Cox, S. R. Brown, T. Ikeda, A. F. May, S. M. Kauzlarich, G. J. Snyder, *Adv. Funct. Mater.* **2008**, *18*, 2795–2800; b) S. R. Brown, S. M. Kauzlarich, F. Gascoin, G. J. Snyder, *Chem. Mater.* **2006**, *18*, 1873–1877.
[12] a) C. Wood, D. Emin, *Phys. Rev. B* **1984**, *29*, 4582–4587; b) C. Wood, D. Emin, P. E. Gray, *Phys. Rev. B* **1985**, *31*, 6811–6814.
[13] a) C. Wood, *Rep. Prog. Phys.* **1988**, *51*, 459–539; b) G. Joshi, H. Lee, Y. Lan, X. Wang, G. Zhu, D. Wang, R. W. Gould, D. C. Cuff, M. Y. Tang, M. S. Dresselhaus, G. Chen, Z. Ren, *Nano Lett.* **2008**, *8*, 4670–4674.
[14] a) H. Ohta, K. Sugiura, K. Koumoto, *Inorg. Chem.* **2008**, *47*, 8429–8436; b) L. Bocher, M. H. Aguirre, D. Logvinovich, A. Shkabko, R. Robert, M. Trottmann, A. Weidenkaff, *Inorg. Chem.* **2008**, *47*, 8077–8085; significantly higher ZT values were reported for some Co oxides; however these data were not reproduced later by other groups, see reference [14a] and discussion therein.
[15] a) T. Mori in *Handbook on the Physics and Chemistry of Rare Earths, Vol. 38* (Eds.: K. A. Gschneidner, Jr., J.-C. Bunzli, V. Pecharsky), North-Holland, Amsterdam, **2008**; b) T. Mori, T. Nishimura, *J. Solid State Chem.* **2006**, *179*, 2908–2915.
[16] B. B. Iversen, A. E. C. Palmqvist, D. E. Cox, G. S. Nolas, G. D. Stucky, N. P. Blake, H. Metiu, *J. Solid State Chem.* **2000**, *149*, 455–458.
[17] M. Falmbigl, P. F. Rogl, E. Bauer, M. Kriegisch, H. Mueller, S. Paschen, *Mater. Res. Soc. Symp. Proc.* **2009**, *1166*, 1166-N06–03.
[18] a) C. L. Condron, S. M. Kauzlarich, T. Ikeda, G. J. Snyder, F. Haarmann, P. Jeglič, *Inorg. Chem.* **2008**, *47*, 8204–8212; b) C. L. Condron, S. M. Kauzlarich, F. Gascoin, G. J. Snyder, *Chem. Mater.* **2006**, *18*, 4939–4945.
[19] K. A. Kovnir, A. V. Shevelkov, *Uspekhi Khimii* **2004**, *73*, 999–1015; K. A. Kovnir, A. V. Shevelkov, *Russ. Chem. Rev.* **2004**, *73*, 923–938.
[20] V. Pacheco, R. Cardoso Gil, Yu. Grin, The 11th European Conference on Solid State Chemistry, Program Schedule and Abstract Book, Caen, **2007**, 194.
[21] A. Saramat, G. Svensson, A. E. C. Palmqvist, C. Stiewe, E. Mueller, D. Platzek, S. G. K. Williams, D. M. Rowe, J. D. Bryan, G. D. Stucky, *J. Appl. Phys.* **2006**, *99*, 023708/1–5.
[22] J. V. Zaikina, K. A. Kovnir, F. Haarmann, W. Schnelle, U. Burkhardt, H. Borrmann, U. Schwarz, Yu. Grin, A. V. Shevelkov, *Chem. Eur. J.* **2008**, *14*, 5414–5422.
[23] a) J. V. Zaikina, K. A. Kovnir, U. Schwarz, H. Borrmann, A. V. Shevelkov, *Z. Kristallogr. New Cryst. Struct.* **2007**, *222*, 177–179; b) K. Kishimoto, T. Koyanagi, K. Akai, M. Matsuura, *Jpn. J. Appl. Phys.* **2007**, *46*, L746–L748; c) F. Philipp, P. Schmidt, *J. Cryst. Growth* **2008**, *310*, 5402–5408; d) J. V. Zaikina, K. A. Kovnir, U. Burkhardt, W. Schnelle, F. Haarmann, U. Schwarz, Yu. Grin, A. V. Shevelkov, *Inorg. Chem.* **2009**, *48*, 3720–3730.
[24] A. Müller, H. Reuter, S. Dillinger, *Angew. Chem.* **1995**, *107*, 2505–2539; *Angew. Chem. Int. Ed. Engl.* **1995**, *34*, 2328–2361.
[25] J. L. Cohn, G. S. Nolas, V. Fessatidis, T. H. Metcalf, G. A. Slack, *Phys. Rev. Lett.* **1999**, *82*, 779–782.
[26] a) J. Nylén, M. Andersson, S. Lidin, U. Häusserman, *J. Am. Chem. Soc.* **2004**, *126*, 16306–16307; b) M. Christensen, B. B. Iversen, *Chem. Mater.* **2007**, *19*, 4896–4905; c) M. Christensen, N. Lock, J. Overgaard, B. B. Iversen, *J. Am. Chem. Soc.* **2006**, *128*, 15657–15665.
[27] J. V. Zaikina, K. A. Kovnir, A. V. Sobolev, I. A. Presniakov, Y. Prots, M. Baitinger, W. Schnelle, A. V. Olenev, O. I. Lebedev, G. Van Tendeloo, Y. Grin, A. V. Shevelkov, *Chem. Eur. J.* **2007**, *13*, 5090–5099.
[28] a) E. M. Vass, M. Hävecker, S. Zafeiratos, D. Teschner, A. Knop-Gericke, R. Schlögl, *J. Phys. Condens. Matter* **2008**, *20*, 184016; b) K. Kovnir, M. Armbrüster, D. Teschner, T. V. Venkov, L. Szentmiklósi, F. C. Jentoft, A. Knop-Gericke, Yu. Grin, R. Schlögl, *Surf. Sci.* **2009**, *603*, 1784–1792.
[29] NIST Electron Inelastic Mean Free Path Database, version 1.1, can be found under http://www.nist.gov/srd/nist71.htm.
[30] J. F. Moulder, W. F. Stickle, P. E. Sobol, K. D. Bomben in *Handbook of X-ray Photoelectron Spectroscopy*, Physical-Electronics, Inc., Eden Prairie, **1995**.
[31] a) A. di Bona, F. Sabary, S. Valeri, P. Michelato, D. Sertore, G. Suberlucq, *J. Appl. Phys.* **1996**, *80*, 3024–3030; b) P. Michelato, C.

Pagani, D. Sertore, A. di Bona, S. Valeri, *Nucl. Instr. Meth. Phys. Res. A* **1997**, *393*, 464–468; c) D. Bisero, A. di Bona, P. Paradisi, S. Valeri, *J. Appl. Phys.* **2000**, *87*, 543–548.

[32] *Chemistry, Structure and Bonding of Zintl Phases and Ions* (Ed.: S. M. Kauzlarich), VCH, Weinheim, **1996**.

[33] J. R. Salvador, C. Malliakas, J. R. Gour, M. G. Kanatzidis, *Chem. Mater.* **2005**, *17*, 1636–1645.

[34] We estimate the contribution from κ_e to the total thermal conductivity by assuming the Wiedemann–Franz relationship. $\kappa_e = L_0 T/\rho$, in which the ideal Lorentz number is taken as $L_0 = 1/3(\pi k_B/e)^2$, while the ρ values were obtained by smoothly extrapolating the resistivity results shown in Figure 5a.

[35] X. Shi, J. Yang, S. Bai, J. Yang, H. Wang, M. Chi, J. R. Salvador, W. Zhang, L. Chen, W. Wong-Ng, *Adv. Funct. Mater.* **2010**, *20*, 755–763.

[36] J. V. Zaikina, W. Schnelle, K. A. Kovnir, A. V. Olenev, Y. Grin, A. V. Shevelkov, *Solid State Sci.* **2007**, *9*, 664–671.

[37] M. Hoelzel, A. Senyshyn, R. Gilles, H. Boysen, H. Fuess, *Neutron News* **2007**, *18*, 23–26.

[38] V. Petricek, M. Dusek, L. Palatinus, JANA2000, Institute of Physics, Academy of Science of the Czech Republic, **2002**.

Received: July 14, 2010
Published online: October 13, 2010

